Dynamic modelling and stability of hingeless helicopter blades with a smart spring

F. F. Afagh, F. Nitzsche and N. Morozova
Department of Mechanical and Aerospace Engineering,
Carleton University,
Ottawa, Canada

ABSTRACT

The aeroelastic stability of a uniform, untwisted hingeless 'smart' helicopter rotor blade in hover has been analysed. The concept of a 'smart' blade is achieved by implementing a piezoelectric stack at an appropriate location along a host blade such that upon actuation it enters the load path becoming an integral part of the host structure. Thus, the stiffness characteristics of the rotor are altered causing modal damping augmentation of the blade. The perturbation equations of motion for the 'smart' blade that describe the unsteady blade motion about the equilibrium operating condition are obtained using Galerkin's method. These differential equations with periodic time coefficients are analysed for stability utilising the Floquet method. Six different regimes of actuation are investigated, and a parametric study is carried out by considering six different design cases. It is shown that, compared to a 'host' blade the stability characteristics of the 'smart' blade are not affected adversely. In fact, a judicious design and actuation of the 'smart' spring has the potential of improving the stability boundaries of individual blades.

NOMENCLATURE

A_i - O_1, B_{xij} - S_{xi}	integrated products of mode shape functions ignoring the 'smart' spring
A	aerofoil lift curve slope
C	blade chord
c_{d_0}	aerofoil profile drag coefficient
E, G	Young's and shear moduli
$[\Delta H(x)]$	Heaviside function
$I_{y'}$, $I_{z'}$	Second area moment of inertia with respect to deformed cross-sectional axes y' and x'
$[\mathbf{I}]$	identity matrix
J	torsional stiffness constant
K, $\bar{m}_{ss}$	non-dimensional parameters
L_u, L_v, L_w, M_ϕ	generalised aerodynamic forces per unit length in the u, v and w directions, respectively and generalised aerodynamic moment
M	mass per unit length
N	frequency of sinusoidal actuation of the 'smart' spring over one rotor revolution of the blade
N	number of non-rotating, uncoupled modes for flap, lead-lag bending and torsion
$[\mathbf{P}]$, $[\mathbf{P}^*(\psi)]$	state space matrices in the perturbation equations
R	length of the blade
$\Re$	flap-lag structural coupling parameter
T	time
T	period of actuation
u, v, w, ϕ	displacements in the x, y, z directions, respectively; torsional displacement about the elastic axis
$[\mathbf{U}]$	matrix of eigenvectors for free vibration case
v_i	induced downwash velocity
V_j, W_j, ϕ_j	lead-lag and flap bending and torsion generalised co-ordinates
V_{0j}, W_{0j}, ϕ_{0j}	lead-lag and flap bending and torsion equilibrium deflections
X	radial co-ordinate
$\{\mathbf{X}\}$	vector of generalised perturbation modal co-ordinates
$Z(x)$	properties of the blade as functions of the radial co-ordinate

Paper No. 2844. Manuscript received 11 June 2003, revised version received 19 April 2004, accepted 7 May 2004.

https://doi.org/10.1017/S0001924000005182 Published online by Cambridge University Press

Z_0, Z_{ss}	properties of the blade corresponding to the blade without/with the 'smart' spring
β_j, γ_j	constants used in the expressions for assumed mode shapes
γ	lock number
ε	small parameter
θ, Ω	blade pitch angle and rotational speed
ψ	azimuth angle (dimensionless time)
ψ_j, $(\bar{x})$, $\Theta(\bar{x})$	non-rotating lead-lag, flap bending and torsional mode shapes
κ	non-dimensional torsional rigidity
Λ_1, Λ_2	non-dimensional bending stiffness with respect to cross-sectional axes
μ, μ_1, μ_2	non-dimensional radii of gyration with respect to cross-sectional axes
ρ_∞	air density
σ	real part of eigenvalue, damping
ω	imaginary part of eigenvalue, frequency
$(\bar{\ })$	refers to non-dimensional quantities
$(\ )_{ss}$	refers to the properties of the 'smart' spring
$(\ )^{na}$, $(\ )^{a}$	refers to the case of non-actuated/actuated 'smart' spring
$(\ )_0$	refers to the properties of the blade without the 'smart' spring

1.0 INTRODUCTION

The noise and vibration experienced inside a helicopter airframe are well recognised as a source of considerable degree of nuisance and discomfort, so that under certain operational conditions, especially for civilian services, the unique mission capabilities of helicopters are not being deployed to their full extent. The inertial and aerodynamic loads acting on the rotor blades induce corresponding reactive loads at the rotor hub, thus resulting in an inherent coupling between the dynamics of the airframe and the rotor. This phenomenon has been identified as a main source contributing to the vibration of the airframe. To address the problem various approaches have been investigated to actively attenuate or control the level of such a forced dynamic response. In this regard, the active control of the vibration characteristics of rotor blade may be considered as a major approach. In general, all efforts to use this approach may be classified in two categories: higher harmonic control (HHC) and individual blade control (IBC). In case of HHC, where all blades are actuated simultaneously through the swashplate by subjecting the rotor to a single higher harmonic, the non-rotating frame attached to the aircraft is used to achieve a time-dependent pitch control of the rotor. In spite of satisfactory results in both theoretical and experimental studies[1-11], the HHC approach has some limitations. At least in comparison with the passive approaches normally employed for attenuation of vibrations the HHC approach requires relatively complicated systems. Also, the additional accessories required for the implementation of this approach are not necessarily negligible weight wise[12]. Moreover, flight tests have indicated that although HHC is capable of reducing the vibration loads at the hub, it does not always result in a similar reduction of vibration level in the airframe. This can be explained by the fact that by applying a HHC to an *N*-blade rotor, one controls only the $(N-1)/rev$, N/rev, and $(N+1)/rev$ frequencies by introducing a single frequency of N/rev to excite the harmonic pitch displacement of the swashplate[13]. On the other hand, using the IBC approach each blade may be controlled individually in the rotating frame attached to the hub, resulting in very efficient reduction in the level of vibration in helicopters[14]. In fact, due to recent developments in adaptive structures technology and its application to helicopter vibration control, the IBC approach has become particularly attractive to the endeavour of developing a true 'smart' rotor. A comprehensive review of the most important research initiatives in this area is found in Ref. 15. The concept of the 'smart' spring is well suited for the IBC approach.

In general, any control strategy associated with an IBC approach can be classified under one of the following two types of control configurations. The first one involves using distributed control configuration. This can be achieved, for example, by embedding the adaptive material in the blade laminate as an integral part of the structure. By actuating the embedded adaptive material one induces strain deformations in the blade that can be controlled externally.

Using this strategy one can take advantage of some of the inherent features of the distributed control theory such as its robustness and superior authority over the degrees of freedom of the system. However, the inability of the adaptive material to induce sufficient strain deformations in the full-scale blade under aerodynamic and inertial loads can be a challenging problem. The second strategy involves using lumped control configuration in which the control is affected on a relatively small segment of the blade. Although this strategy can be prone to spillover problems, yet it has a better capability to overcome the work done by typical aerodynamic and inertia loads that the blade encounters during flight. The concept of the 'smart' spring affords a lumped parameter control approach.

Helicopter rotors that are presently manufactured by the rotorcraft industry can have configurations with various degrees of articulation ranging from fully 'articulated' to 'hingeless' rotors, with semi-rigid rotors and gimballed rotors as other examples. The articulated blade, in which the bending moments at the root are eliminated, requires relatively complicated mechanical design at the hinge connection of the blade to the rotor hub. With developments in advanced composite materials in recent years, the new trend has been to develop a hingeless blade by eliminating hinges at the blade root connection to the hub. The hingeless configuration is mechanically simpler and is also of particular interest due to the fact that it affords an increased controllability. However, due to the nonlinear coupling that occurs between the three modes of flap, lead-lag and torsional motions of the cantilever blade, it can become susceptible to instability problems unless detailed attention is paid to the design and analysis of the blade to minimise the destabilising effect of such coupling. In fact, the stability problem of conventional hingeless rotor blades are reasonably well understood and considerable work has been devoted to the investigation of this problem, with the result that successful hingeless rotor systems are currently used by the industry[16-24]. However, implementation of a smart device in a hingeless host blade and its actuation will change the dynamic characteristics of the blade, and therefore, the dynamic stability of the resulting 'smart' blade needs to be investigated. In an attempt to address precisely this issue, the present study outlines a procedure to investigate the corresponding eigenvalue problem in order to determine whether inclusion of a 'smart' spring and its actuation-de-actuation will affect the dynamic stability of an initially stable blade in an adverse manner.

2.0 'SMART' SPRING CONCEPT

The development of a smart device that can oppose the effects of typical aerodynamic loads acting on rotor blades during flight is an ongoing challenge. While smart materials with adequate dynamic response such as electrostrictive and magnetostrictive materials, or piezoelectric crystal PZT and film PVDF can deliver relatively large forces they are characterised by inadequate displacement capability. Although the stroke of these materials can be improved in various ways, for example, by using stacked piezoelectric actuators, this is always accompanied by a trade-off in the actuation force. Other smart materials such as shape memory alloys that can deliver sufficient actuation power suffer from poor bandwidth and inadequate dynamic response. Some recent endeavours to develop integrated active fibre composites by embedding piezoelectric fibres in the composite host structure have shown a good potential of applicability of this approach in full size blades.

https://doi.org/10.1017/S0001924000005182 Published online by Cambridge University Press

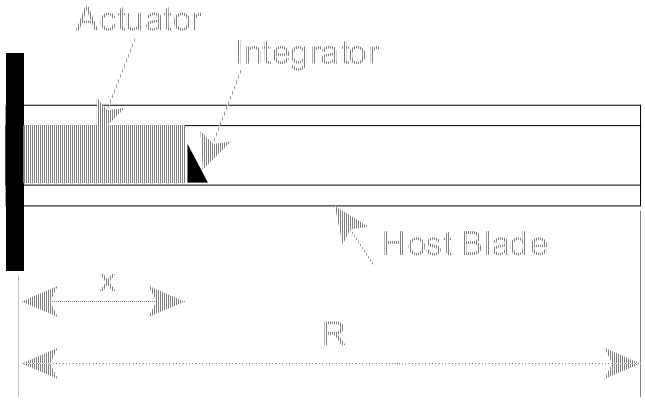


Figure 1. The concept of 'smart' spring.

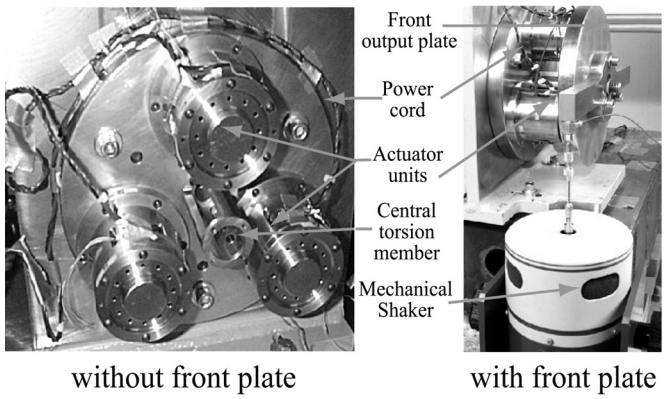


Figure 2. Torsional 'smart' spring tested at the NRC laboratories in Ottawa, Canada.

The concept of the 'smart' spring upon which the present work is based, exploits the limited stroke of piezoelectric materials in conjunction with their large force, stiffness and bandwidth to achieve aeroelastic control by dynamically controlling the cross-section properties of the rotor blade[25-30]. A conceptual arrangement of the device is shown in Fig. 1, where the host beam is augmented by inclusion of an actuator as a 'smart spring' at the root. By inducing micro displacements, but large forces, sufficiently high friction forces can develop between the host structure and the actuator so that the actuator enters the load path as an integral part of the host structure changing the torsional as well as bending stiffness of the cross-section. Large actuation forces accompanied by small strokes mean that relatively small mechanical work is required to achieve full control authority. The activation-deactivation of the device changes various stiffnesses of the blade accordingly. For example, as the result of a periodic actuation of the device, during the first half of a cycle stiffnesses of the section increase to their maximum value, while during the second half, as the actuator is disengaged, the stiffnesses are reduced to their original baseline values of the host structure.

A prototype of the device that is designed to actuate in the torsional degree of freedom, has been undergoing preliminary proof-of-concept tests at the Aeroacoustics and Structural Dynamics, Structures, Materials and Propulsion Laboratory of the National Research Council of Canada, Fig. 2. This experimental setup used three stacked PZT actuator cans that are integrated as additional structural components into the load path by means of induced frictional forces. This results in a change in the torsional stiffness of the blade at the root, which in turn affects the aeroelastic response of the blade. A central torsion member closely duplicates the stiffness of the baseline blade. Accelerometers along the blade sense the vibration data that is fed to the control computer for signal analysis and system identification to generate the proper control signal to the actuators to attenuate vibration. In the corresponding wind tunnel tests a vortex generator was used to simulate the unsteady aerodynamic loads that a blade would be subjected to. The results indicate promising capability for the smart spring to reduce the vibration levels where the base-line condition at a 50Vdc applied voltage is depicted as 100% vibration, Fig. 3.

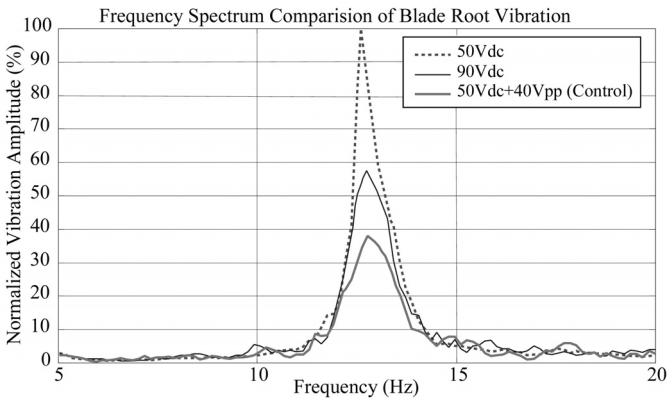


Figure 3. Wind-tunnel test results to evaluate the capability of the 'smart spring' for IBC application under unsteady aerodynamic loading (nonrotating blade section).

3.0 DYNAMIC MODEL OF THE 'SMART' BLADE

The governing differential equations of motion for a long, non-uniform, straight, slender, homogeneous, isotropic blade with variable twist, pre-cone angle, and a chord-wise symmetric cross-section were developed by Hodges and Dowell[23]. The moderate blade displacements of the elastic axis are denoted by an axial deformation $u(x,t)$, lead-lag bending $v(x,t)$, flap bending $w(x,t)$, and the torsion deformation $\phi(x,t)$ of the cross-section about the elastic axis.

In the present work, any chordwise offsets between the elastic, tension, mass and aerodynamic centre axes were assumed to be absent. This assumption eliminates the possibility of unfavourable relative positioning of these axes which is a primary cause of the type of instability that is characterised by coupled flap-torsion deflections with a frequency near the torsion natural frequency. As the result, the more specific instability of cantilever blade, characterised by the coupled flap, lead-lag and torsion deflections with a frequency near the lead-lag bending natural frequency can be better isolated for investigation. Following the approach based on Hamilton's variational principle as outlined by Hodges and Dowell[23], and Hodges and Ormiston[24], an aeroelastic model was developed for the 'smart' blade under hover conditions in the present work.

To accommodate the implementation of the 'smart' spring in the host blade, all the mass, geometric and elastic parameters of the 'smart' blade are considered to be discontinuous functions of the radial co-ordinate, x, so that any such parameter is expressed as:

$$Z(x) = Z_0 + \Delta H(x) Z_{ss} \quad \ldots (1)$$

where Z_0 represents the parameter's value for the host blade, Z_{ss} is the incremental value of the parameter due to the 'smart' spring, and

https://doi.org/10.1017/S0001924000005182 Published online by Cambridge University Press

$H(x)$ is the Heaviside function. A list of these parameters is given as Equations (A.1) in the Appendix. The new nonlinear, integro-partial differential equations that model the dynamics of the aeroelastic behaviour of the 'smart' blade are obtained by setting the coefficients of arbitrary, admissible variations δu, δv, δw and $\delta\phi$ in Hamilton's integrand equal to zero. The resulting dynamic model is further simplified by substitution to eliminate the axial deformation, $u(x,t)$, and tension as dependent variables. These equations read as follows:

δv equation:

$$
\begin{aligned}
&-\frac{m_0\Omega^2}{2}\left[\left(R^2-x^2\right)v'\right]'-m_{ss}\Omega^2\left[v'\int_x^R\Delta H(x)x\,dx\right]'-2m_0\Omega\left[v'\int_x^R\dot{v}\,dx\right]'\\
&-2m_{ss}\Omega\left[v'\int_x^R\Delta H(x)\dot{v}\,dx\right]'+[((EI_{z'})_0-(EI_{y'})_0)[\frac{\mathrm{Sin}(2\Re\theta)}{2}+\phi\mathrm{Cos}(2\Re\theta)]\,w''\\
&+\Delta H(x)((EI_{z'})_{ss}-(EI_{y'})_{ss})\left[\frac{\mathrm{Sin}(2\Re\theta)}{2}+\phi\mathrm{Cos}(2\Re\theta)\right]w''+[(EI_{z'})_0(\mathrm{Cos}^2(\Re\theta)\\
&-\phi\mathrm{Sin}(2\Re\theta))+(EI_{y'})_0(\mathrm{Sin}^2(\Re\theta)+\phi\mathrm{Sin}(2\Re\theta))]\,v''+\Delta H(x)[(EI_{z'})_{ss}(\mathrm{Cos}^2(\Re\theta)\\
&-\phi\mathrm{Sin}(2\Re\theta))+(EI_{y'})_{ss}(\mathrm{Sin}^2(\Re\theta)+\phi\mathrm{Sin}(2\Re\theta))]\,v''\}''\\
&-2\Omega(m_0+\Delta H(x)m_{ss})\int_0^x(\dot{v}'v'+\dot{w}'w')\mathrm{d}x+(m_0+\Delta H(x)m_{ss})(\ddot{v}-\Omega^2v)=L_v
\end{aligned}
\qquad \ldots (2.1)
$$

δw equation:

$$
\begin{aligned}
&-\frac{m_0\Omega^2}{2}\left[\left(R^2-x^2\right)w'\right]'-m_{ss}\Omega^2\left[w'\int_x^R\Delta H(x)x\,dx\right]'-2m_0\Omega\left[w'\int_x^R\dot{v}\,dx\right]'\\
&-2m_{ss}\Omega\left[w'\int_x^R\Delta H(x)\dot{v}\,dx\right]'+\{((EI_{z'})_0-(EI_{y'})_0)[\frac{\mathrm{Sin}(2\Re\theta)}{2}+\phi\mathrm{Cos}(2\Re\theta)]\,v''\\
&+\Delta H(x)((EI_{z'})_{ss}-(EI_{y'})_{ss})[\frac{\mathrm{Sin}(2\Re\theta)}{2}+\phi\mathrm{Cos}(2\Re\theta)]\,v''+[(EI_{z'})_0(\mathrm{Sin}^2(\Re\theta)\\
&+\phi\mathrm{Sin}(2\Re\theta))+(EI_{y'})_0(\mathrm{Cos}^2(\Re\theta)-\phi\mathrm{Sin}(2\Re\theta))]\,w''+\Delta H(x)[(EI_{z'})_{ss}(\mathrm{Sin}^2(\Re\theta)\\
&+\phi\mathrm{Sin}(2\Re\theta))+(EI_{y'})_{ss}(\mathrm{Cos}^2(\Re\theta)-\phi\mathrm{Sin}(2\Re\theta))]\,w''\}''+(m_0+\Delta H(x)m_{ss})\ddot{w}=L_w
\end{aligned}
\qquad \ldots (2.2)
$$

$\delta\phi$ equation:

$$
\begin{aligned}
&-\left\{(GJ)_0\phi'+\Delta H(x)(GJ)_{ss}\phi'\right\}'-\left\{\left((k_A^2)_0+\Delta H(x)(k_A^2)_{ss}\right)\phi'\frac{m_0\Omega^2}{2}\left(R^2-x^2\right)\right\}'\\
&+\left\{\left((k_A^2)_0+\Delta H(x)(k_A^2)_{ss}\right)\phi'm_{ss}\Omega^2\int_x^R\Delta H(x)x\mathrm{d}x\right\}'\\
&+\left((EI_{z'})_0-(EI_{y'})_0\right)\left(w''^2-v''^2\right)\frac{\mathrm{Sin}(2\Re\theta)}{2}+v''w''\mathrm{Cos}(2\Re\theta)]\\
&+\Delta H(x)\left((EI_{z'})_{ss}-(EI_{y'})_{ss}\right)[(w''^2-v''^2)\frac{\mathrm{Sin}(2\Re\theta)}{2}\\
&+v''w''\mathrm{Cos}(2\Re\theta)]+(m_0+\Delta H(x)m_{ss})\left((k_m^2)_0+\Delta H(x)(k_m^2)_{ss}\right)\ddot{\phi}\\
&+(m_0+\Delta H(x)m_{ss})\Omega^2\phi\left[(k_{m2}^2)_0-(k_{m1}^2)_0+\Delta H(x)\left((k_{m2}^2)_{ss}-(k_{m1}^2)_{ss}\right)\right]\mathrm{Cos}(2\theta)\\
&=M_\phi-(m_0+\Delta H(x)m_{ss})\Omega^2[(k_{m2}^2)_0-(k_{m1}^2)_0+\Delta H(x)\{(k_{m2}^2)_{ss}-(k_{m1}^2)_{ss}\}]\frac{\mathrm{Sin}(2\theta)}{2}
\end{aligned}
\qquad \ldots (2.3)
$$

In Equation (2), L_v, and L_w represent the in-plane and out-of-plane aerodynamic loads acting per unit length of the blade, respectively, with M_ϕ being the aerodynamic pitching moment per unit length. These are obtained using Greenberg's extension of Theodorson's theory for a two dimensional aerofoil that is subjected to sinusoidal motion in pulsating incompressible flow[31]. The corresponding aerodynamic loads for hover conditions can be obtained using strip theory in which only the velocity component perpendicular to the blade spanwise axis is considered in formulating the aerodynamic forces. A quasi-steady approximation of the unsteady theory for low reduced frequency is used. Moreover, classical blade element-momentum theory is used to calculate the steady induced inflow for the rotor. These simplifying assumptions are considered to be reasonable for low frequency stability analysis of a rotor in hover[24].

4.0 PERTURBATION EQUATIONS OF MOTION

Using Galerkin's method Equations (2) can be reduced to a set of ordinary nonlinear differential equations. To this end, these equations are first non-dimensionalised. Then the corresponding non-dimensional displacements are prescribed as a product series of generalised co-ordinates and mode shape functions as:

$$
\begin{aligned}
\bar{v}&=\sum_{j=1}^{N}V_j(\psi)\Psi_j(\bar{x}),\\
\bar{w}&=\sum_{j=1}^{N}W_j(\psi)\Psi_j(\bar{x}),\\
\phi&=\sum_{j=1}^{N}\phi_j(\psi)\Theta_j(\bar{x})
\end{aligned}
\qquad \ldots (3)
$$

where, for a blade with radius R and rotor angular velocity of Ω the non-dimensional parameters $\bar{x}=x/R$, $\bar{v}=v/R$, $\bar{w}=w/R$ and $\psi=\Omega t$ are defined. The eigenfunctions of a non-rotating cantilever beam are used as the sets of linearly independent comparison functions ψ_j, Θ_j while V_j, W_j and ϕ_j are the generalised co-ordinates of the problem. As the final result, Equations (2) are reduced into a set of $3N$ nonlinear, ordinary differential equations in terms of the generalised co-ordinates V_j, W_j and ϕ_j:

δv equations:

$$
\begin{aligned}
&\sum_{j=1}^{N}\Big\langle V_j\{D_{ij}+\bar{m}_{ss}D_{xij}+[\Lambda_{02}-(\Lambda_{02}-\Lambda_{01})\mathrm{Sin}^2(\Re\theta)]\beta_j^4\delta_{ij}-(\delta_{ij}+\bar{m}_{ss}\delta_{xij1})\\
&+[\Lambda_{ss2}-(\Lambda_{ss2}-\Lambda_{ss1})\mathrm{Sin}^2(\Re\theta)]\Delta_{xij1}\}+W_j\frac{\mathrm{Sin}(2\Re\theta)}{2}\{(\Lambda_{02}-\Lambda_{01})\beta_j^4\delta_{ij}\\
&+(\Lambda_{ss2}-\Lambda_{ss1})\Delta_{xij1}\}+(\Lambda_{02}-\Lambda_{01})\sum_{k=1}^{N}K_{jki}\phi_j\left[W_k\mathrm{Cos}(2\Re\theta)-V_k\mathrm{Sin}(2\Re\theta)\right]\\
&+(\Lambda_{ss2}-\Lambda_{ss1})\sum_{k=1}^{N}K_{xjki}\phi_j\left[W_k\mathrm{Cos}(2\Re\theta)-V_k\mathrm{Sin}(2\Re\theta)\right]\\
&+2\sum_{k=1}^{N}\left(F_{ikj}-F_{jki}+\bar{m}_{ss}(F_{xikj}-F_{xjki})\right)V_k\dot{V}_j-2\sum_{k=1}^{N}(F_{jki}+\bar{m}_{ss}F_{xjki})W_k\dot{W}_j+(\delta_{ij}+\bar{m}_{ss}\delta_{xij1})\ddot{V}_j\\
&+\frac{\gamma}{6}[\bar{v}_iI_{ij}\phi_j+\left(2\frac{c_{d0}}{a}E_{ij}+\theta\bar{v}_i\delta_{ij}+\bar{v}_i\sum_{k=1}^{N}\phi_kH_{ijk}\right)\dot{V}_j-\left(2\bar{v}_i\delta_{ij}-\theta E_{ij}-\sum_{k=1}^{N}\phi_kG_{ijk}\right)\dot{W}_j]\Big\rangle\\
&=\frac{\gamma}{6}[\bar{v}_i^2A_i-\frac{c_{d0}}{a}C_i-\bar{v}_i\theta B_i],\qquad i=1,\ldots,N
\end{aligned}
\qquad \ldots (4.1)
$$

δw equations:

$$
\begin{aligned}
&\sum_{j=1}^{N}\Big\langle V_j\frac{\mathrm{Sin}(2\Re\theta)}{2}[(\Lambda_{02}-\Lambda_{01})\beta_j^4\delta_{ij}+(\Lambda_{ss2}-\Lambda_{ss1})\Delta_{xij1}]+W_j\{D_{ij}+\bar{m}_{ss}D_{xij}\\
&+[\Lambda_{01}+(\Lambda_{02}-\Lambda_{01})\mathrm{Sin}^2(\Re\theta)]\beta_j^4\delta_{ij}+[\Lambda_{ss1}+(\Lambda_{ss2}-\Lambda_{ss1})\mathrm{Sin}^2(\Re\theta)]\Delta_{xij1}\}\\
&+(\Lambda_{02}-\Lambda_{01})\sum_{k=1}^{N}K_{jki}\phi_j[V_k\mathrm{Cos}(2\Re\theta)+W_k\mathrm{Sin}(2\Re\theta)]\\
&+(\Lambda_{ss2}-\Lambda_{ss1})\sum_{k=1}^{N}K_{xjki}\phi_j\left[V_k\mathrm{Cos}(2\Re\theta)+W_k\mathrm{Sin}(2\Re\theta)\right]\\
&+2\sum_{k=1}^{N}(F_{ikj}+\bar{m}_{ss}F_{xikj})W_k\dot{V}_j+\ddot{W}_j(\delta_{ij}+\bar{m}_{ss}\delta_{xij1})+\frac{\gamma\bar{c}}{24}\ddot{W}_j\delta_{ij}\\
&+\frac{\gamma}{6}[-J_{ij}\phi_j+\sum_{k=1}^{N}L_{ijk}V_jW_k-\frac{\bar{c}}{2}O_{ij}W_j-(2\theta E_{ij}+2\sum_{k=1}^{N}\phi_kG_{ijk}-\bar{v}_i\delta_{ij})\dot{V}_j+E_{ij}\dot{W}_j-\frac{3\bar{c}}{4}I_{ij}\phi_j]\Big\rangle\\
&=\frac{\gamma}{6}[-\bar{v}_iB_i+\theta C_i],\qquad i=1,\ldots,N
\end{aligned}
\qquad \ldots (4.2)
$$

$\delta\phi$ equations:

$$
\begin{aligned}
&\sum_{j=1}^{N}\Big\langle\phi_j[\mu_0^2K_0N_{ij}+\mu_0^2\bar{m}_{ss}KP_{xij}+\mu_{ss}^2K_{ss}Q_{xij}+\mathrm{i}\,{}^2_{ss}\bar{m}_{ss}K_{ss}R_{xij}\\
&+[\kappa_0\gamma_j^2+(\mu_{02}^2-\mu_{01}^2)\mathrm{Cos}(2\theta)]\delta_{ij}+\kappa_{ss}\gamma_j^2\delta_{xij2}+(\mu_{ss2}^2-\mu_{ss1}^2\\
&+\bar{m}_{ss}(\mu_{02}^2-\mu_{01}^2)+\bar{m}_{ss}(\mu_{ss2}^2-\mu_{ss1}^2))\mathrm{Cos}(2\theta)\delta_{xij2}]\\
&+(\Lambda_{02}-\Lambda_{01})\sum_{k=1}^{N}K_{ijk}[\mathrm{Cos}(2\Re\theta)V_jW_k+\frac{\mathrm{Sin}(2\Re\theta)}{2}(W_jW_k-V_jV_k)]\\
&+(\Lambda_{ss2}-\Lambda_{ss1})\sum_{k=1}^{N}K_{xijk}[\mathrm{Cos}(2\Re\theta)V_jW_k+\frac{\mathrm{Sin}(2\Re\theta)}{2}(W_jW_k-V_jV_k)\\
&+\frac{\gamma\bar{c}^2}{48}M_{ij}\ddot{\phi}_j+(\mu_0^2\delta_{ij}+\mu_{ss}^2\delta_{xij2}+\bar{m}_{ss}\mu_0^2\delta_{xij2}+\bar{m}_{ss}\mu_{ss}^2\delta_{xij2})\ddot{\phi}_j\Big\rangle
\end{aligned}
\qquad \ldots (4.3)
$$

https://doi.org/10.1017/S0001924000005182 Published online by Cambridge University Press

$$= -S_{xi}(\mu_{ss2}^2 - \mu_{ss1}^2 + \bar{m}_{ss}(\mu_{02}^2 - \mu_{01}^2) + \bar{m}_{ss}(\mu_{ss2}^2 - \mu_{ss1}^2))\frac{\mathrm{Sin}(2\theta)}{2}$$

$$-(\mu_{02}^2 - \mu_{01}^2)\frac{\mathrm{Sin}(2\theta)}{\sqrt{2}\gamma_i}, \quad i = 1,\ldots,N$$

The Galerkin integrals and the non-dimensional parameters appearing in Equations (4) are given in Appendix A as Equations (A.2.1) and (A.2.2), respectively.

Then, the generalised co-ordinates can be expressed as a combination of steady-state quantities that represent the dynamics of equilibrium or trim conditions and small perturbations, i.e.,

$$\begin{aligned} V_j(\psi) &= V_{0j} + \Delta V_j(\psi) \\ W_j(\psi) &= W_{0j} + \Delta W_j(\psi) \\ \phi_j(\psi) &= \phi_{0j} + \Delta\phi_j(\psi) \end{aligned} \quad \ldots (5)$$

Upon substituting the steady-state quantities into Equation (4) these equations are rendered to a set of 3*N* non-linear, algebraic equations of equilibrium. The solution of this set results in the modal amplitudes of the trim condition. A second set of equations is available from the substitution of Equation (5) into the 3N nonlinear, ordinary differential equations of motion given by Equation (4). Subtracting the first set of equilibrium equations from this second set of equations and neglecting all the non-linear products of the perturbation quantities yields a set of 3*N* homogeneous linear differential equations on the perturbation quantities:

$$\begin{Bmatrix} \dot{\mathbf{X}} \\ \ddot{\mathbf{X}} \end{Bmatrix} = \begin{bmatrix} [0] & [I] \\ -[\mathbf{M}+\Delta\mathbf{M}]^{-1}[\mathbf{K}+\Delta\mathbf{K}(\psi)] & -[\mathbf{M}+\Delta\mathbf{M}]^{-1}[\mathbf{C}+\Delta\mathbf{C}] \end{bmatrix} \begin{Bmatrix} \mathbf{X} \\ \dot{\mathbf{X}} \end{Bmatrix} = [\mathbf{P}] \begin{Bmatrix} \mathbf{X} \\ \dot{\mathbf{X}} \end{Bmatrix} \quad \ldots (6)$$

where,

$$\{\mathbf{X}\} = \{\Delta V_1 \ \ldots \ \Delta V_N \ \ \Delta W_1 \ \ldots \ \Delta W_n \ \ \Delta\phi_1 \ \ldots \ \Delta\phi_N\}^T \quad \ldots (7)$$

and [**M**], [**C**], and [**K**] represent the mass, damping and stiffness matrices, respectively, due to the host blade, while [Δ**M**], [Δ**C**], and [Δ**K**] are the mass, damping and stiffness matrices, respectively, due to the 'smart' spring. Detailed expressions for these matrices are given in Appendix A, Equations (A.3-A.5). Using a so-called principle co-ordinate transformation, the eigenvectors' matrix [**U**] of the free vibration of the undamped host blade with the eigenvectors corresponding to the higher frequencies removed, can be used to reduce the size of matrix [**P**] in Equations (6) without significantly affecting the eigenvalues. As the result, the perturbation Equations (6) read:

$$\begin{Bmatrix} \dot{\mathbf{X}} \\ \ddot{\mathbf{X}} \end{Bmatrix} = \begin{bmatrix} [0] & [I] \\ -[\mathbf{M}_m]^{-1}[\mathbf{K}_k(\psi)] & -[\mathbf{M}_m]^{-1}[\mathbf{C}_C] \end{bmatrix} \begin{Bmatrix} \mathbf{X} \\ \dot{\mathbf{X}} \end{Bmatrix} = [\mathbf{P}^*(\psi)] \begin{Bmatrix} \mathbf{X} \\ \dot{\mathbf{X}} \end{Bmatrix} \quad \ldots (8)$$

where

$$\begin{aligned} [\mathbf{M}_m] &= [\mathbf{U}]^T[\mathbf{M}+\Delta\mathbf{M}][\mathbf{U}] \\ [\mathbf{C}_C] &= [\mathbf{U}]^T[\mathbf{C}+\Delta\mathbf{C}][\mathbf{U}] \\ [\mathbf{K}_k(\psi)] &= [\mathbf{U}]^T[\mathbf{K}+\Delta\mathbf{K}(\psi)][\mathbf{U}]. \end{aligned} \quad \ldots (9)$$

A periodic actuation of the 'smart' spring results in a periodic variation of the geometric and cross-sectional stiffness of the 'smart' blade. Considering a sinusoidal variation in time with a period of $2\pi/n$ where n is the number of actuation-de-actuations during one rotation of the blade, in terms of the non-dimensionalised time, i.e., the azimuth angle $\psi = \Omega t$, the dimensionless period of actuation becomes $T = 2\pi/n$. The mathematical representation of varying parameters is:

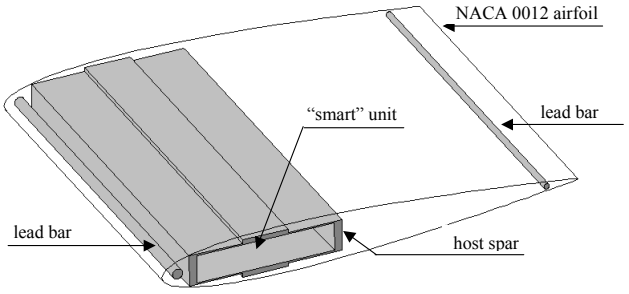


Figure 4. 'Smart' blade design.

$$\mathbf{Z}_{ss}(\psi) = \frac{\mathbf{Z}_{ss}^{a} + \mathbf{Z}_{ss}^{na}}{2} + \frac{\mathbf{Z}_{ss}^{a} - \mathbf{Z}_{ss}^{na}}{2}\ \mathrm{Sin}(n\psi) \quad \ldots (10)$$

where superscript $(\,)^a$ corresponds to the case of constant actuation of the 'smart' spring, while $(\,)^{na}$ refers to the case of non-actuated spring. Hence, in Equations (8) and (9) the matrix [Δ**K**(**ψ**)] is a function of the non-dimensional time or azimuth, **ψ**. Therefore, perturbation Equations (8) are, in fact, linear ordinary differential equations with periodic coefficients that can be solved for the stability using Floquet method. In applying the Floquet method, the '*n*-pass method' was used to numerically integrate the equations of motion in order to obtain the corresponding transition matrix[12,32].

5.0 STABILITY ANALYSIS AND DISCUSSION OF RESULTS

A realistic analysis requires using configuration parameters of an actual blade. To this end, a Eurocopter BO105 helicopter blade was considered in this work. In anticipation of future experimental work, a reduced scale model of this blade with a radius of two metres was designed. This model includes a single aluminium spar that has a single cell rectangular cross-section and is embedded within non-structural foam as shown in Fig. 3.

A non-structural skin cover applied around the foam completes the chord-wise symmetric model of the corresponding NACA 0012 aerofoil. The mass centre of the blade was designed to be at the quarter point of the chord from the leading edge by including proper mass-tuning lead bars near the leading and trailing edges of the aerofoil.

The 'smart' spring is located inside the spar cell and extends along the radius of the blade for a distance x measured from the root, Fig. 1. An examination of the maximum deflection of a cantilever beam when subjected to a uniformly distributed external static load indicates that, for a given length of an actuated 'smart' spring, the tip deflection of the blade will decrease as the 'smart' spring is placed closer to the blade root.

A parametric investigation was carried out to determine the significance of various parameters from the stability point of view. The parameters that were considered to be of significant importance for this purpose were: the length of the 'smart' spring, the blade pitch angle θ, and the structural coupling parameter ℜ. Two different lengths of the 'smart' spring were considered. These were 15% and 5% of the blade length. The pitch angle was taken to range from its baseline value of zero to 0·3 radians. The structural coupling parameter ℜ represents the influence of the relative bending stiffness of the inboard and outboard blade segments on the flap-lag and bending-torsional coupling[24]. Two extreme cases, representing full flap-lag structural coupling, ℜ = 1, and no flap-lag coupling, ℜ = 0, were considered. Finally, in reference to Fig. 1, upon actuation of the spring, the bending stiffness of the blade for a length x is modelled

https://doi.org/10.1017/S0001924000005182 Published online by Cambridge University Press

Table 1
Design cases

Case No	$\Re$	x/R (%)	Shear deflection
1	0	15	Yes
2	1	15	Yes
3	0	15	No
4	1	15	No
5	0	5	Yes
6	0	5	No

in terms of an equivalent host spar that would result in the same static deflection as the actuated blade. Two separate approaches were used in this modelling. In the first approach the strain energy due to only bending, and hence, deflections due to only bending were considered. In the second approach the strain energy due to transverse shear was also included, and hence, deflections due to both bending and transverse shear were considered. Thus, the six design cases shown in Table 1 were investigated.

Moreover, six different 'regimes' representing various configurations of the blade structure and 'smart' spring actuation schemes were analysed. These regimes were:

1. Conventional baseline blade (CBB): representing the conventional BO-105 blade consisting only of the host aluminium spar.
2. Smart baseline blade (SBB): represents the CBB structure that includes a non-actuated 'smart' spring.
3. Direct current: represents the SBB regime in which the 'smart' spring is subjected to a DC current.
4-6. Alternating currents (AC3), (AC4), and (AC5): represent the SBB regime in which the 'smart' spring is actuated sinusoidally at three, four, and five cycles of actuation-de-actuation per one rotor revolution, respectively.

Each of the six design cases tabulated in Table 1 was subjected to the six different regimes that are outlined above. In each case the stability of the first four modes, i.e. the first lead-lag, first and second flap and first torsion modes was studied. The root loci of each of the first four modes were determined for values of pitch angle between zero and 0·3 radians. In general, each root is a complex number whose real part represents the corresponding modal damping with the imaginary part being the modal frequency. In order to investigate the results, in each case, the modal damping and frequencies are presented as functions of the pitch angle. Figs. 5-7 show the corresponding results for design case 4, as typical illustration of the results. In these diagrams a positive damping at a nonzero frequency indicates the onset of flutter instability, whereas, a positive damping associated with a zero frequency is indicative of divergence type of instability.

6.0 CONCLUSIONS

Based on the results obtained from stability investigation of the six different design cases, each being subjected to six different actuation regimes, the following general conclusions are obtained. In this outline, the motion of the blade is considered stable if all the modes

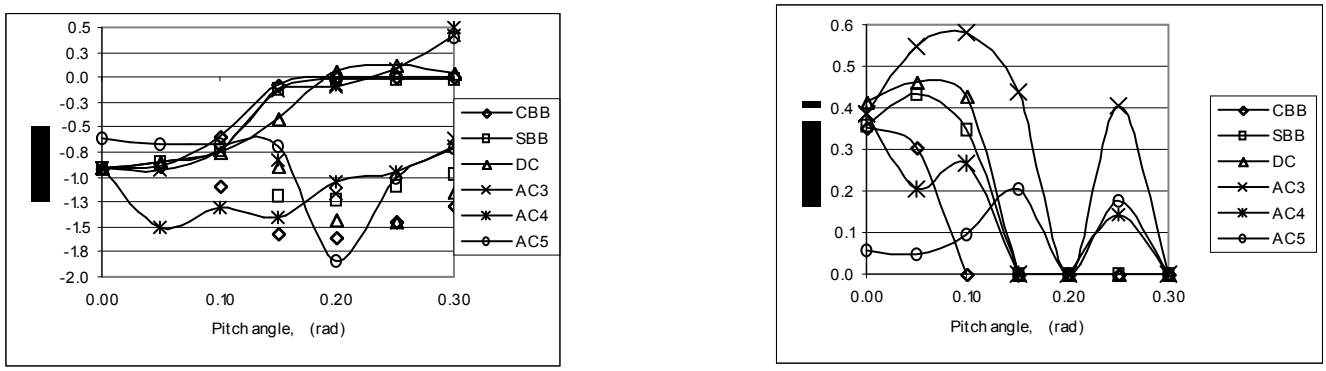


Figure 5. Design case 4: Damping and frequency of the first lead-lag mode.

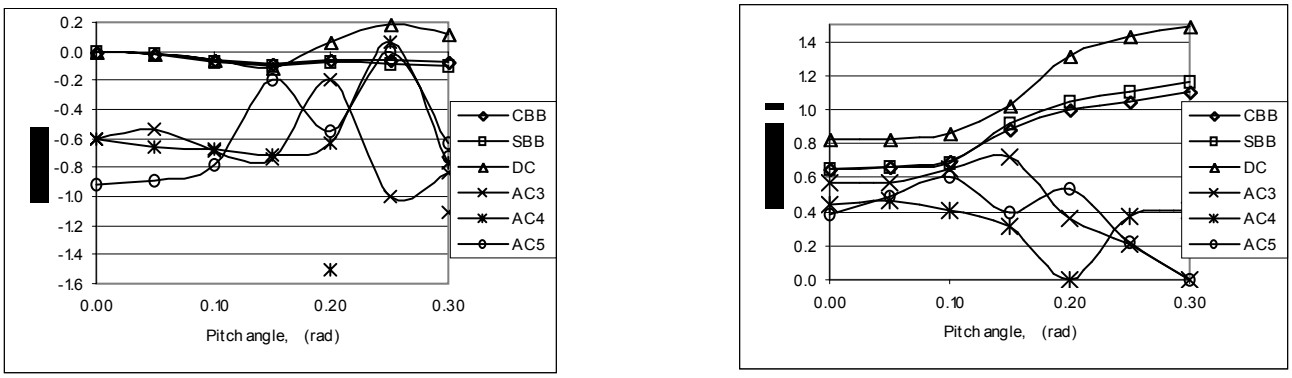


Figure 6. Design case 4: Damping and frequency of the first flap mode.

https://doi.org/10.1017/S0001924000005182 Published online by Cambridge University Press

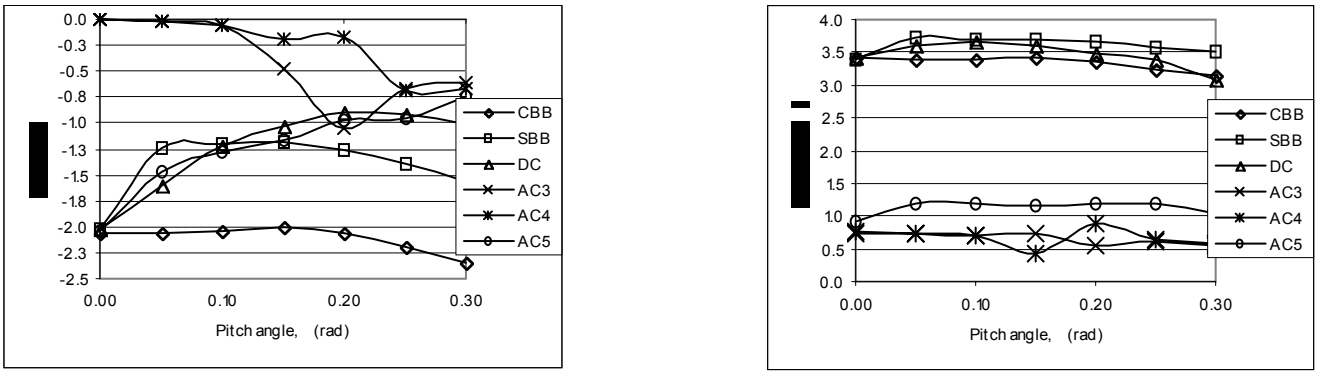


Figure 7. Design case 4: Damping and frequency of the first torsion mode.

that were considered, behaved in a stable manner, otherwise the blade is considered to be unstable:

- The stability of motion of a 'smart' rotor blade when subjected to parametric excitation is investigated. The parametric excitation used is a harmonic one, and is caused by periodic engaging and disengaging of a 'smart' device which results in a periodic modification of the elastic stiffness of the blade.
- In general, for most of the practical operational range of pitch angles, i.e. $\theta < 0{\cdot}25$rad, compared to a 'host' blade, the stability characteristics of the 'smart' blade are not affected adversely. In fact, for a judicious design an appropriate periodic actuation of the 'smart' spring can augment the stability characteristic of the fundamental modes of the smart blade. Compared to a conventional 'host' blade, it is possible to improve the stability boundary of a 'smart' blade by as much as 200% in one of the design cases studied.
- The length of the 'smart' spring that is to be used is an important design consideration. In general, a longer spring, reflecting a longer length of blade whose elastic stiffnesses are affected by the actuation, results in blades with higher frequencies, especially, at lower pitch angles.
- In comparison to no flap-lag coupling, i.e., when $\Re = 0$, in the presence of full flap-lag coupling, i.e., for $\Re = 1$, the 'smart' blade can become unstable at relatively lower pitch angles.
- In modelling the structural stiffness of the smart blade, neglecting the effect of shear strain affects the prediction of stability limits. This becomes a more pronounced factor when designing for shorter lengths of 'smart' spring.

REFERENCES

1. CHOPRA, I. and MCCLOUD, J.L. A numerical simulation study of open-loop, closed-loop and adaptive multicycle control systems, *J Amer Heli Soc*, 1983, **28**, (1), pp 63-77.
2. JACOB, H.G. and LEHMANN, G. Optimization of blade pitch angle for higher harmonic rotor control, *Vertica*, 1983, **7**, (3), pp 271-286.
3. HAMMON, C.E. Wind tunnel results showing rotor vibration loads reduction using higher harmonic blade pitch, *J Amer Heli Soc*, 1983, **28**, (1), pp 10-15.
4. MOLUSIS, J.A., HAMMOND, C.E. and CLINE, J.H. A unified approach to the optimal design of adaptive and gain scheduled controllers to achieve minimum helicopter vibration, *J Amer Heli Soc*, 1983, **28**, (2), pp 9-18.
5. WOOD, E.R., POWERS, R., CLINE, J.H. and HAMMOND, C.E. On developing and flight testing a higher harmonic control system, *J Amer Heli Soc*, 1985, **30**, (1), pp 3-20.
6. LEHMANN, G. The effect of higher harmonic control (HHC) on a four-bladed hingeless model rotor, *Vertica*, 1985, **9**, (3), pp 273-284.
7. ACHACTE, M. and POLYCHRONIADIS, M. Development of an experimental system for active control of vibration in helicopters – development methodology for an airborne system, *Vertica*, 1987, **11**, (1/2), pp 123-138.
8. SHAW, J., ALBION, N., HANKER, E.J. and TEAL, R.S. Higher harmonic control: wind tunnel demonstration of fully effective vibratory hub force suppression, *J Amer Heli Soc*, 1989, **34**, (1), pp. 14-25.
9. NGUYEN, K. and CHOPRA, I. Application of higher harmonic control (HHC) to hingeless rotor systems, 1989, proceedings of the AIAA/ASME/ASCE/AHS/ASC 30th Structures, Structural Dynamics, and Materials Conference, Part I, AIAA, Washington, DC, pp 507-520.
10. ROBINSON, L.H. and FRIEDMAN, P.P. Analytical simulation of higher harmonic control using a new aeroelastic model, 1989, proceedings of the AIAA/ASME/ASCE/AHS/ASC 30th Structures, Structural Dynamics, and Materials Conference, Part 3, AIAA, Washington, DC, pp 1394-1406.
11. KUBE, R. Aeroelastic effects of helicopter vibration reduction by higher harmonic control, 1991, proceedings of the International Forum on Aeroelasticity and Structural Dynamics, German Society for Aeronautics and Astronautics (DGLR), Bonn, Germany, pp 496-504.
12. BIELAWA, R.L. *Rotary Wing Structural Dynamics and Aeroelasticity*, 1992, AIAA Education Series, PREZEMIENIECKI, J.S. (Ed).
13. NITZSCHE, F. and BREITBACH, E.J. Using adaptive structures to attenuate rotary wing aeroelastic response, *J Aircr*, 1994, **31**, (5), pp 1178-1188.
14. NITZSCHE, F. A comparative study on different techniques to control rotary wing vibration using smart structures, *Aeronaut J*, 1999, **103**, (1027), pp 429-434.
15. CHOPRA, I. Development of a smart rotor, 1993, proceedings of 19th European Rotorcraft Forum, Associazione Italiana di Aeronautica Ed Astronautica, Cernobbio, Italy, pp N6.1-N6.18.
16. HOUBOLT, J.C. and BROOKS, G.W. Differential equations of motion for combined flapwise bending, chordwise bending, and torsion of twisted, nonuniform rotor blades, 1958, NACA Report 1346, pp 179-195
17. YOUNG, M.I. A theory of rotor blade motion stability in powered flight, *J Amer Heli Soc*, 1964, **9**, (3), pp 12-25.
18. MIL, M.L., NEKRASOV, A.V., BRAVERMAN, A.S. GRODLKO, L.N. and LEYKAND, M.A., Helicopters, calculation and design, *Aerodynamics*, 1967, **1**, NASA TT F-494.
19. ARCIDIACONO, P.J. Prediction of rotor instability at high forward speeds, steady flight differential equations of motion for a flexible helicopter blade with chordwise mass unbalance, 1969, USAAVLABS TR 68-18A.
20. ORMISTON, R.A. and HODGES, D.H. Linear flap-lag dynamics of hingeless helicopter rotor blades in hover, *J Amer Heli Soc*, 1972, **17**, (2), pp 2-14.
21. FRIEDMAN, P. and TONG, P. Dynamic nonlinear elastic stability of helicopter rotor blades in hover and forward flight, 1972, ASRL-TR-116-3, Massachusetts Institute of Technology, NAS2-6175, NASAR 114485.
22. HODGES, D.H. and ORMISTON, R.A. Stability of elastic bending and torsion of uniform cantilevered rotor blades in hover, 1973, proceedings of the AIAA/ASME/ASCE/AHS/ASC 14th Structures, Structural Dynamics, and Materials Conference, Williamsburg, Virginia, AIAA Paper 73-105.

https://doi.org/10.1017/S0001924000005182 Published online by Cambridge University Press

23. HODGES, D.H. and DOWELL, E.H. Nonlinear equations of motion for the elastic bending and torsion of twisted nonuniform rotor blades, 1974, NASA TN D-7818.
24. HODGES, D.H. and ORMISTON, R.A. Stability of elastic bending and torsion of uniform cantilever rotor blades in hover with variable structural coupling, 1976, NASA TN D-8192
25. NITZSCHE, F., GREWAL, A. and ZIMCIK, D. Structural component having means for actively varying its stiffness to control vibration, 1999, U.S. Patent No 5 973 440. European Patent EP-996570 -B1.
26. NITZSCHE, F. Aeroelastic analysis of a rotor blade with active impedance control at the root, *Canadian Aeronautics and Space J*, 2001, **47**, (1).
27. YOUNG, C. and ZIMCIK, D.G., WICKRAMASINGHE, V.K. and NITZSCHE, F. Development of the smart spring active vibration control of helicopter blades, *J Intelligent Material Systems and Structures* (accepted for publication 2003).
28. NITZSCHE, F., ZIMCIK, D., WICKRAMASINGHE, V. and YONG, C. Control laws for an active tunable vibration absorber designed for aeroelastic damping augmentation, *Aeronaut J*, January 2004, **108**, (1079), pp 35-42.
29. NITZSCHE, F., HAROLD, T., WICKRAMASINGHE, V.K., YOUNG, C. and ZIMCIK, D.G. Development of a maximum energy extraction control for the smart spring, 2003, proceedings 14th International Conference on Adaptive Structures and Technology, 7-9 October 2003, Seoul, Korea (to be published).
30. NITZSCHE, F., SOLAIMAN, S. and AFAGH, F. Smart blade effects on the aeroelastic characteristics of helicopter rotors, 1999, proceedings of CEAS Forum on Aeroacoustics of Rotors and Propellers, Rome, Italy, 9-11 June 1999, pp 119-131.
31. GREENBERG, J.M. Airfoil in sinusoidal motion in a pulsating stream, 1947, NACA TN-1326.
32. MOROZOVA, N. Dynamic Stability Analysis of a Helicopter Blade with Adaptive Damper, 2002, MSc thesis, Dept of Mechanical and Aerospace Engineering, Carleton University, Ottawa, Canada.

APPENDIX A

The mass and cross-section parameters used in Equations (2) are:

$$m(x) = m_0 + \Delta H(x) m_{ss}$$

$$A(x) = A_0 + \Delta H(x) A_{ss}$$

$$I_{y'}(x) = (I_{y'})_0 + \Delta H(x)(I_{y'})_{ss}$$

$$I_{z'}(x) = (I_{z'})_0 + \Delta H(x)(I_{z'})_{ss}$$

$$J(x) = J_0 + \Delta H(x) J_{ss}$$

$$k_A^2(x) = (k_A^2)_0 + \Delta H(x)(k_A^2)_{ss}$$

$$k_{m1}^2(x) = (k_{m1}^2)_0 + \Delta H(x)(k_{m1}^2)_{ss}$$

$$k_{m2}^2(x) = (k_{m2}^2)_0 + \Delta H(x)(k_{m2}^2)_{ss} \qquad \ldots \text{(A.1)}$$

$$(k_m^2(x))_{ss} = (k_{m1}^2)_{ss} + (k_{m2}^2)_{ss}$$

$$m_{ss} = \iint_{A_{ss}} \rho_{ss}\, d\eta\, d\zeta$$

$$A_{ss} = \iint_{A_{ss}} d\eta\, d\zeta$$

$$(I_{y'})_{ss} = \iint_{A_{ss}} \zeta^2\, d\eta\, d\zeta$$

$$(I_{z'})_{ss} = \iint_{A_{ss}} \eta^2 d\eta d\zeta$$

$$J_{ss} = (I_{y'})_{ss} + (I_{z'})_{ss}$$

$$(k_A^2)_0 = \frac{1}{A_0} \iint_{A_0} (\eta^2 + \zeta^2)\, d\eta\, d\zeta$$

$$k_A^2 = \frac{1}{A_0 + A_{ss}} \iint_{A_0 + A_{ss}} (\eta^2 + \zeta^2)\, d\eta\, d\zeta$$

$$(k_{m1}^2)_0 = \frac{1}{m_0} \iint_{A_0} \rho\zeta^2\, d\eta\, d\zeta$$

$$k_{m1}^2 = \frac{1}{m_0 + m_{ss}} \iint_{A_0 + A_{ss}} \rho\zeta^2\, d\eta\, d\zeta$$

$$(k_{m2}^2)_0 = \frac{1}{m_0} \iint_{A_0} \rho\eta^2\, d\eta\, d\zeta$$

$$k_{m2}^2 = \frac{1}{m_0 + m_{ss}} \iint_{A_0 + A_{ss}} \rho\eta^2\, d\eta\, d\zeta$$

The Galerkin integrals used in Equation (4) are:

$$A_i = \int_0^1 \Psi_i \, d\bar{x}$$

$$B_i = \int_0^1 \bar{x} \Psi_i \, d\bar{x}$$

$$C_i = \int_0^1 \bar{x}^2 \Psi_i \, d\bar{x}$$

$$D_{ij} = \int_0^1 \frac{1 - \bar{x}^2}{2} \Psi_i' \Psi_j' \, d\bar{x}$$

$$E_{ij} = \int_0^1 \bar{x} \Psi_i \Psi_j \, d\bar{x}$$

$$I_{ij} = \int_0^1 \bar{x} \Psi_i \Theta_j \, d\bar{x}$$

$$J_{ij} = \int_0^1 \bar{x}^2 \Psi_i \Theta_j \, d\bar{x}$$

$$M_{ij} = \int_0^1 \bar{x} \Theta_i \Theta_j \, d\bar{x}$$

$$N_{ij} = \int_0^1 \frac{1 - \bar{x}^2}{2} \Theta_i' \Theta_j' \, d\bar{x}$$

$$O_{ij} = \int_0^1 \bar{x} \Psi_i \Psi_j' \, d\bar{x}$$

$$\delta_{ij} = \int_0^1 \Psi_i \Psi_j \, d\bar{x} = \int_0^1 \Theta_i \Theta_j \, d\bar{x} = \begin{cases} 0; & i \neq j \\ 1; & i = j \end{cases} \qquad \ldots \text{(A.2.1)}$$

$$F_{ijk} = -\frac{1}{\beta_k^4} \int_0^1 \Psi_i' \Psi_j' \Psi_k''' \, d\bar{x}$$

$$G_{ijk} = \int_0^1 \bar{x} \Psi_i \Psi_j \Theta_k \, d\bar{x}$$

$$H_{ijk} = \int_0^1 \Psi_i \Psi_j \Theta_k \, d\bar{x}$$

$$K_{ijk} = \int_0^1 \Theta_i \Psi_j'' \Psi_k'' \, d\bar{x}$$

$$L_{ijk} = \int_0^1 \bar{x} \Psi_i \Psi_j \Psi_k' \, d\bar{x} - \int_0^1 \bar{x}^2 \Psi_i \left(\int_0^{\bar{x}} \Psi_j'(\bar{x}) \Psi_k''(\bar{x}) d\bar{x} \right) d\bar{x}$$

$$\delta_{xij1} = \int_{\bar{x}_1}^{\bar{x}_2} \Psi_i \Psi_j \, d\bar{x}$$

$$\delta_{xij2} = \int_{\bar{x}_1}^{\bar{x}_2} \Theta_i \Theta_j \, d\bar{x}$$

$$\Delta_{xij1} = \int_{\bar{x}_1}^{\bar{x}_2} \Psi_i'' \Psi_j'' \, d\bar{x}$$

$$P_{xij} = \int_{\bar{x}_1}^{\bar{x}_2} \frac{\bar{x}_2^2 - \bar{x}^2}{2} \Theta_i' \Theta_j' \, d\bar{x} + \int_0^{\bar{x}_1} \frac{\bar{x}_2^2 - \bar{x}_1^2}{2} \Theta_i' \Theta_j' \, d\bar{x}$$

https://doi.org/10.1017/S0001924000005182 Published online by Cambridge University Press

$$Q_{xij} = \int_{\bar{x}_1}^{\bar{x}_2} \frac{1-\bar{x}^2}{2} \Theta_i' \Theta_j' \, d\bar{x}$$

$$R_{xij} = \int_{\bar{x}_1}^{\bar{x}_2} \frac{\bar{x}_2^2 - \bar{x}^2}{2} \Theta_i' \Theta_j' \, d\bar{x}$$

$$K_{xijk} = \int_{\bar{x}_1}^{\bar{x}_2} \Theta_i \Psi_j'' \Psi_k'' \, d\bar{x}$$

$$S_{xi} = \int_{\bar{x}_1}^{\bar{x}_2} \Theta_i d\bar{x}$$

$$B_{xi} = \int_{\bar{x}_1}^{\bar{x}_2} \bar{x} \Psi_i d\bar{x}$$

The non-dimensional parameters used in Equations (4) are:

$$K_0 = \frac{(k_A^2)_0}{(k_m^2)_0} \qquad K_{ss} = \frac{(k_A^2)_{ss}}{(k_m^2)_{ss}}$$
$$\mu_0 = \frac{(k_m)_0}{R} \qquad \mu_{ss1} = \frac{(k_{m1})_{ss}}{R}$$
$$\Lambda_{01} = \frac{(EI_{y'})_0}{m_0 \Omega^2 R^4} \qquad \Lambda_{02} = \frac{(EI_{z'})_0}{m_0 \Omega^2 R^4}$$
$$\kappa_0 = \frac{(GJ)_0}{m_0 \Omega^2 R^4} \qquad \kappa_{ss} = \frac{(GJ)_{ss}}{m_0 \Omega^2 R^4} \qquad \ldots (A.2.2)$$
$$\mu_{01} = \frac{(k_{m1})_0}{R} \qquad \mu_{02} = \frac{(k_{m2})_0}{R}$$
$$\mu_{ss2} = \frac{(k_{m2})_{ss}}{R} \qquad \mu_{ss} = \frac{(k_m)_{ss}}{R}$$
$$\Lambda_{ss1} = \frac{(EI_{y'})_{ss}}{m_0 \Omega^2 R^4} \qquad \Lambda_{ss2} = \frac{(EI_{z'})_{ss}}{m_0 \Omega^2 R^4}$$
$$\gamma = \frac{3\rho_\infty acR}{m_0} \qquad \bar{m}_{ss} = \frac{m_{ss}}{m_0}$$

The mass damping and stiffness matrices in Equations (6) are:

$$[\mathbf{M}] = \begin{bmatrix} \delta_{ij} & 0 & 0 \\ 0 & \delta_{ij}\left(1+\frac{\gamma \bar{c}}{24}\right) & 0 \\ 0 & 0 & \mu^2 \delta_{ij} \end{bmatrix} \qquad \ldots (A.3.1)$$

$$[\Delta \mathbf{M}] = \begin{bmatrix} \bar{m}_{ss}\delta_{xij1} & 0 & 0 \\ 0 & \bar{m}_{ss}\delta_{xij1} & 0 \\ 0 & 0 & (\mu_{ss}^2 + \bar{m}_{ss}\mu_0^2 + \bar{m}_{ss}\mu_{ss}^2)\delta_{xij2} \end{bmatrix} \qquad \ldots (A.3.2)$$

$$[\mathbf{C}] = 2\begin{bmatrix} \sum_{k=1}^{N}(F_{ikj} - F_{jki})V_{0k} & -\sum_{k=1}^{N} F_{jki} W_{0k} & 0 \\ \sum_{k=1}^{N} F_{ikj} W_{0k} & 0 & 0 \\ 0 & 0 & 0 \end{bmatrix}$$

$$\begin{bmatrix} (2\frac{c_{d0}}{a}E_{ij} + \theta\bar{v}_i\delta_{ij} + \bar{v}_i\sum_{k=1}^{N} H_{ijk}\phi_{0k}) & (-2\bar{v}_i\delta_{ij} + \theta E_{ij} + \sum_{k=1}^{N} G_{ijk}\phi_{0k}) & 0 \\ (-2\theta E_{ij} + \bar{v}_i\delta_{ij} - 2\sum_{k=1}^{N} G_{ijk}\phi_{0k}) & E_{ij} & -\frac{3\bar{c}}{4} I_{ij} \\ 0 & 0 & \frac{\bar{c}^2}{8} M_{ij} \end{bmatrix} \qquad \ldots (A.4.1)$$

$$[\Delta \mathbf{C}] = 2\begin{bmatrix} \bar{m}_{ss}\sum_{k=1}^{N}(F_{xikj} - F_{xjki})V_{0k} & -\bar{m}_{ss}\sum_{k=1}^{N} F_{xjki} W_{0k} & 0 \\ \bar{m}_{ss}\sum_{k=1}^{N} F_{xikj} W_{0k} & 0 & 0 \\ 0 & 0 & 0 \end{bmatrix} \qquad \ldots (A.4.2)$$

$$[\mathbf{K}] = \begin{bmatrix} K_{11}^s & K_{12}^s & K_{13}^s \\ K_{21}^s & K_{22}^s & K_{23}^s \\ K_{31}^s & K_{32}^s & K_{33}^s \end{bmatrix} + \frac{\gamma}{6}\begin{bmatrix} K_{11}^a & K_{12}^a & K_{13}^a \\ K_{21}^a & K_{22}^a & K_{23}^a \\ K_{31}^a & K_{32}^a & K_{33}^a \end{bmatrix} \qquad \ldots (A.5.1)$$

where,

$$\begin{aligned}
(K_{11}^s)_{ij} &= D_{ij} + \left[\Lambda_2 - (\Lambda_2 - \Lambda_1)\mathrm{Sin}^2(\Re\theta)\right]\beta_j{}^4\delta_{ij} - \delta_{ij} - \\
&\quad - (\Lambda_2 - \Lambda_1)\sum_{k=1}^{N} K_{kji}\phi_{0k}\mathrm{Sin}(2\Re\theta) \\
(K_{12}^s)_{ij} &= (\Lambda_2 - \Lambda_1)\frac{\mathrm{Sin}(2\Re\theta)}{2}\beta_j{}^4\delta_{ij} + (\Lambda_2 - \Lambda_1)\sum_{k=1}^{N} K_{kji}\phi_{0k}\mathrm{Cos}(2\Re\theta) \\
(K_{13}^s)_{ij} &= (\Lambda_2 - \Lambda_1)\sum_{k=1}^{N} K_{jki}[\mathrm{Cos}(2\Re\theta)W_{0k} - \mathrm{Sin}(2\Re\theta)V_{0k}] \\
(K_{21}^s)_{ij} &= (\Lambda_2 - \Lambda_1)\frac{\mathrm{Sin}(2\Re\theta)}{2}\beta_j{}^4\delta_{ij} + (\Lambda_2 - \Lambda_1)\sum_{k=1}^{N} K_{kji}\phi_{0k}\mathrm{Cos}(2\Re\theta) \\
(K_{22}^s)_{ij} &= D_{ij} + \left[\Lambda_1 + (\Lambda_2 - \Lambda_1)\mathrm{Sin}^2(\Re\theta)\right]\beta_j{}^4\delta_{ij} + \\
&\quad + (\Lambda_2 - \Lambda_1)\sum_{k=1}^{N} K_{kji}\phi_{0k}\mathrm{Sin}(2\Re\theta) \\
(K_{23}^s)_{ij} &= (\Lambda_2 - \Lambda_1)\sum_{k=1}^{N} K_{jki}[\mathrm{Cos}(2\Re\theta)V_{0k} + \mathrm{Sin}(2\Re\theta)W_{0k}] \\
(K_{31}^s)_{ij} &= (\Lambda_2 - \Lambda_1)\sum_{k=1}^{N} K_{ijk}[-\mathrm{Sin}(2\Re\theta)V_{0k} + \mathrm{Cos}(2\Re\theta)W_{0k}] \\
(K_{32}^s)_{ij} &= (\Lambda_2 - \Lambda_1)\sum_{k=1}^{N} K_{ijk}[\mathrm{Cos}(2\Re\theta)V_{0k} + \mathrm{Sin}(2\Re\theta)W_{0k}]
\end{aligned} \qquad \ldots (A.5.2)$$

$$[\Delta \mathbf{K}] = \begin{bmatrix} \Delta K_{11} & \Delta K_{12} & \Delta K_{13} \\ \Delta K_{21} & \Delta K_{22} & \Delta K_{23} \\ \Delta K_{31} & \Delta K_{32} & \Delta K_{33} \end{bmatrix} \qquad \ldots (A.5.3)$$

$$\begin{aligned}
(\Delta K_{11})_{ij} &= \bar{m}_{ss}(D_{xij} - \delta_{xij1}) + \left[\Lambda_{ss2} - (\Lambda_{ss2} - \Lambda_{ss1})\mathrm{Sin}^2(\Re\theta)\right]\Delta_{xij1} \\
&\quad - (\Lambda_{ss2} - \Lambda_{ss1})\sum_{k=1}^{N} K_{xkji}\phi_{0k}\mathrm{Sin}(2\Re\theta) \\
(\Delta K_{12})_{ij} &= (\Lambda_{ss2} - \Lambda_{ss1})\sum_{k=1}^{N} K_{xkji}\phi_{0k}\mathrm{Cos}(2\Re\theta) + (\Lambda_{ss2} - \Lambda_{ss1})\Delta_{xij1}\frac{\mathrm{Sin}(2\Re\theta)}{2} \\
(\Delta K_{13})_{ij} &= (\Lambda_{ss2} - \Lambda_{ss1})\sum_{k=1}^{N} K_{xjki}[W_{0k}\mathrm{Cos}(2\Re\theta) - V_{0k}\mathrm{Sin}(2\Re\theta)] \\
(\Delta K_{21})_{ij} &= (\Lambda_{ss2} - \Lambda_{ss1})\sum_{k=1}^{N} K_{xkji}\phi_{0k}\mathrm{Cos}(2\Re\theta) + (\Lambda_{ss2} - \Lambda_{ss1})\Delta_{xij1}\frac{\mathrm{Sin}(2\Re\theta)}{2} \\
(\Delta K_{22})_{ij} &= (\Lambda_{ss2} - \Lambda_{ss1})\sum_{k=1}^{N} K_{xkji}\phi_{0k}\mathrm{Sin}(2\Re\theta) + \bar{m}_{ss} D_{xij} \\
&\quad + \left[\Lambda_{ss1} + (\Lambda_{ss2} - \Lambda_{ss1})\mathrm{Sin}^2(\Re\theta)\right]\Delta_{xij1} \\
(\Delta K_{23})_{ij} &= (\Lambda_{ss2} - \Lambda_{ss1})\sum_{k=1}^{N} K_{xjki}[V_{0k}\mathrm{Cos}(2\Re\theta) + W_{0k}\mathrm{Sin}(2\Re\theta)] \\
(\Delta K_{31})_{ij} &= (\Lambda_{ss2} - \Lambda_{ss1})\sum_{k=1}^{N} K_{xijk}[-V_{0k}\mathrm{Sin}(2\Re\theta) + W_{0k}\mathrm{Cos}(2\Re\theta)] \\
(\Delta K_{32})_{ij} &= (\Lambda_{ss2} - \Lambda_{ss1})\sum_{k=1}^{N} K_{xijk}[V_{0k}\mathrm{Cos}(2\Re\theta) + W_{0k}\mathrm{Sin}(2\Re\theta)] \\
(\Delta K_{33})_{ij} &= \mu_0^2 \bar{m}_{ss} KP_{xij} + \mu_{ss}^2 K_{ss} Q_{xij} + \mu_{ss}^2 \bar{m}_{ss} K_{ss} R_{xij} \\
&\quad + \kappa_{ss}\gamma_j^2\delta_{xij2} + (\mu_{ss2}^2 - \mu_{ss1}^2 + \bar{m}_{ss}(\mu_{02}^2 - \mu_{01}^2) + \bar{m}_{ss}(\mu_{ss2}^2 - \mu_{ss1}^2))\mathrm{Cos}(2\theta)\delta_{xij2}
\end{aligned} \qquad \ldots (A.5.4)$$

https://doi.org/10.1017/S0001924000005182 Published online by Cambridge University Press